

Energy barriers and cooperative motion at the surface of freestanding glassy polystyrene films

D. Fujimoto,^{1,2, a)} W. A. MacFarlane,^{2,3,4} and J. Rottler^{1,2, b)}

¹⁾*Department of Physics and Astronomy, University of British Columbia, Vancouver, BC V6T 1Z1, Canada*

²⁾*Stewart Blusson Quantum Matter Institute, University of British Columbia, Vancouver, BC V6T 1Z4, Canada*

³⁾*Department of Chemistry, University of British Columbia, Vancouver, BC V6T 1Z1, Canada*

⁴⁾*TRIUMF, Vancouver, BC V6T 2A3, Canada*

(Dated: 18 June 2022)

We investigate the near-surface relaxation of freestanding atactic polystyrene films with molecular dynamics simulations. As in previous coarse-grained simulations, relaxation times for backbone segments and phenyl rings are linked to their bulk relaxation times via a power law coupling relation. Variation of the coupling exponent with distance from the surface is consistent with depth-dependent activation barriers. We also quantify a reduction of dynamical heterogeneity at the interface which can be interpreted in the framework of cooperative models for glassy dynamics.

I. INTRODUCTION

Polymers have a high degree of mechanical and chemical tunability, making them extremely versatile materials. Upon cooling, many polymers vitrify rather than crystallize. Long before a crystal forms, molecular motion becomes frozen and dynamical timescales quickly surpass those accessible in experiments. Boundary conditions have a strong impact on these relaxation dynamics in glassy polymers¹. In freestanding films with a vacuum interface, the glass transition temperature, T_g , is reduced as the thickness decreases^{2,3}. Moreover, the layer-resolved segmental (relaxation) dynamics accelerates substantially as the depth z below the free interface decreases^{4–7}. Recent evidence from molecular dynamics simulation (MD)⁸ and theoretical arguments⁹ suggest that the molecular relaxation time $\tau(z, T)$ near the surface is coupled to the bulk relaxation time $\tau_b(T)$ via a power-law relation

$$\tau(z, T) \sim \tau_b(T)^{f(z)}, \quad (1)$$

with a “coupling exponent” $f(z) \in [0, 1]$ capturing the dependence on depth z . The origin of this power-law form, as explained below, lies in the exponential dependence of the relaxation time on an energetic barrier for activated motion.

Several theoretical pictures have been proposed that arrive at the same functional form eq. (1), but differ in their interpretation of the coupling exponent. The “elastically collective nonlinear Langevin equation” (ECNLE) theory of Schweizer and co-workers¹⁰, for instance, proposes a reduction of the activation barrier via modified local caging constraints due to loss of neighbors as well

as truncation of long range elastic interactions^{11–14}. Another picture asserts that the coupling exponent reflects a temperature and distance-dependent reduction of the size of string-like cooperative mobile regions as the major driver of interfacial relaxation¹⁵. A recent study by Zhang, Starr, and Douglas¹⁶, however, indicates that the length of such mobile strings varies only weakly near the interface, although the dynamical scale of this layer¹⁷ is proportional to the length of mobile strings^{18,19}. Gaps thus remain in our understanding of interfacial dynamics of glass-forming materials.

The present study presents MD simulations of freestanding atactic polystyrene (PS) films at the united-atom level. It builds on previous results of Zhou and Milner²⁰, who computed the layer-resolved segmental relaxation times in PS-films of up to 28 nm thickness by monitoring the angular displacement along the polymer backbone (see Figure 1). Here we focus additionally on the rotational dynamics of the phenyl sidegroups that reflect (slightly faster) γ -relaxation processes²¹. The phenyl ring motion is particularly important for the interpretation of β -detected nuclear magnetic resonance (β -NMR) experiments, because the Li^+ -ions are expected to be bound between such rings^{7,22}. We determine the coupling exponent that describes the dynamics at the surface, and show that its functional form is consistent with an average activation barrier that varies with depth. We also compute, as one measure of cooperativity, the dynamical four-point susceptibility $\chi_4(T, z, t)$, and find that it decreases strongly at the surface. A coupling exponent based on this parameter can therefore also describe the observed variation of relaxation times with depth.

^{a)} Electronic mail: fujimoto@phas.ubc.ca

^{b)} Electronic mail: jrottler@physics.ubc.ca

II. DESCRIPTIONS OF INTERFACIAL DYNAMICS

A. Distance dependent energy barrier

In polymeric glass formers, the temperature dependence of the bulk relaxation time typically exhibits thermally activated behavior, which is well-described over some range of T by the Vogel-Fulcher-Tammann (VFT) equation. In a film, it is reasonable to expect that the barrier for activated motion, as well as the exponential prefactor, become explicitly dependent on the depth z , such that the VFT equation reads

$$\tau(z, T) = \tau_0(z) \exp \left[\frac{\Delta E(z)}{k_B(T - T_0)} \right], \quad (2)$$

where T_0 denotes the Vogel temperature, and the effective activation energy barrier $\Delta E(z)$ reflects an average over a distribution of local energy barriers for molecular motion. The bulk relaxation time is $\tau_b(T) = \tau(\infty, T)$. After dividing by $\tau_b(T)$, equation (2) can be rearranged as

$$\frac{\ln(\tau(z, T)/\tau_0(z))}{\ln(\tau_b(T)/\tau_0)} = \frac{\Delta E(z)}{\Delta E_\infty} = f(z), \quad (3)$$

or alternatively

$$\frac{\tau(T, z)}{\tau_0(z)} = \left(\frac{\tau_b(T)}{\tau_0} \right)^{f(z)}. \quad (4)$$

This simple heuristic derivation yields a coupling relation between bulk and surface dynamics with a temperature-independent coupling exponent as introduced by Diaz-Vela, Hung, and Simmons⁸. It can be expected to hold below an onset temperature where $\tau_b(T) \gg \tau_0 \equiv \tau_0(\infty)$ and the interfacial dynamics “decouples” from the bulk and becomes faster. At higher temperatures, however, the coupling exponent $f(z) \simeq 1$ and the interfacial dynamics is strongly coupled to the bulk. Simulations for vacuum interfaces suggest that below the onset temperature the coupling exponent is temperature-independent and has an exponential depth-dependence, $f(z) = 1 - \epsilon_0 \exp(-z/\xi_{\Delta E})$ with $\xi_{\Delta E}$ an interfacial length scale⁸.

B. Cooperative strings

An alternative approach posits that the origin of the enhanced surface relaxation is a reduction of the number of particles involved collectively in a structural relaxation event. It builds on the well established observation (mainly from simulations) that mobile particles in glasses organize themselves in a string-like form such that $N^*(T)$ particles have to relax for one particle to escape from a local cage. Salez *et al.*¹⁵ start from a free volume picture and write the probability for an N -particle

relaxation process along a string in the bulk:

$$P_N(T) \sim \frac{1}{\lambda^3 \tau_c} \epsilon^{N-1} (1 - \epsilon) \theta(N - N^*(T)), \quad (5)$$

where τ_c is an ‘onset’ timescale, λ an average intermolecular distance, and $\epsilon = \tau_0/\tau_c \ll 1$ is an elementary ‘coherence probability’. Since particles in a cooperative string need to move in phase, one expects the probability to decrease exponentially with the string length. The total probability for relaxation,

$$P(T) = \sum_{N=N^*}^{\infty} P_N(T) \sim \frac{1}{\lambda^3 \tau_c} \epsilon^{N^*-1}, \quad (6)$$

is dominated by the threshold string length N^* . Defining the bulk relaxation time as $\tau_b(T) \sim 1/P(T)$, one obtains

$$\frac{\tau_b(T)}{\tau_0} \sim \left(\frac{\tau_c}{\tau_0} \right)^{N^*(T)}. \quad (7)$$

Salez *et al.*¹⁵ now generalize this expression for the bulk relaxation time to free interfaces by replacing $N^*(T)$ with $N^*(z, T) = N^*(T) f(z/\xi_b(T))$ where $f(z/\xi_b(T)) \leq 1$ reflects a reduction of the length of the cooperative string near the surface. This reduction can be expected to occur over a scale set by the temperature-dependent bulk cooperative length scale $\xi_b(T)$. Interestingly, this yields a formula for the relaxation times near free interfaces that has the same form as eq. (4),

$$\frac{\tau(T, z)}{\tau_0} = \left(\frac{\tau_b(T)}{\tau_0} \right)^{f(z, T)}, \quad (8)$$

but the coupling exponent now reads

$$f(z, T) = \frac{N^*(z, T)}{N^*(T)} \quad (9)$$

and depends explicitly on temperature. Moreover, τ_0 is assumed to be independent of position and just reflects a microscopic timescale. The fact that the same functional form arises in two seemingly independent derivations can be traced to the exponential dependence of the probability for relaxation on the size of the cooperative region. The model thus embodies the central tenet of the Adam-Gibbs argument, namely that the activation barrier is proportional to the number of particles in the cooperatively rearranging region. The string model of (bulk) glassy dynamics²³ makes this explicit,

$$\tau(T) \propto [\exp(\Delta\mu/k_B T)]^{f(T)} \quad (10)$$

with $f(T) = L(T)/L(T_A)$, where $L(T)$ is the length of the cooperative string and $\Delta\mu$ is the activation barrier at an onset temperature T_A .

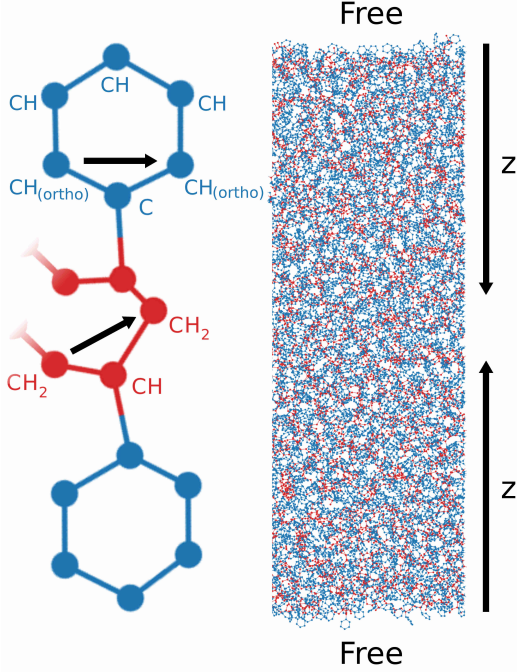


FIG. 1. Snapshot of a simulated free-standing atactic polystyrene film at $T = 200$ K. The distance between the two surfaces is about 31 nm. Vectors connecting ortho-atoms and adjacent CH_2 united atoms on the backbone are used to measure the polymer dynamics.

III. SIMULATION METHODS

A united atom model of atactic PS introduced previously by Vorselaars, Lyulin, and Michels²¹ was used to simulate free standing films ~ 30 nm thick. The $\sim 4 \times 10^4$ atom simulation was composed of 500 polymer chains, each 10 monomer units in length. Molecular dynamics simulations were carried out using the LAMMPS package²⁴ in an NVT ensemble with a Nosé-Hoover thermostat. The equations of motion were integrated with a time step of 2 fs in a velocity-Verlet scheme. Periodic boundaries were used along both \hat{x} and \hat{y} , and reflective walls were used along \hat{z} , with final box dimensions fixed to $5.5 \times 5.5 \times 40$ nm. To prevent drift, the center of mass linear momentum was re-scaled to zero at every time step.

The film was generated by placing the polymer chains in a $40 \times 40 \times 40$ nm simulation box and equilibrating at 600 K for 5 ns, accommodating for placement overlap by limiting atomic motion to 0.1 Å for the first 10 ps. The box was then compressed to its final dimensions over 10 ns. After another 5 ns, the reflective walls were relaxed to their initial positions over the course of 10 ns, and an additional 5 ns was allowed to pass. The film was then cooled at 0.01 K ps^{-1} , which is a typical rate used in MD^{20,21}. The glass transition temperature T_g of the film was found to be 395(4) K using the density, and 405(3) K using the film height (Figure 2), where the

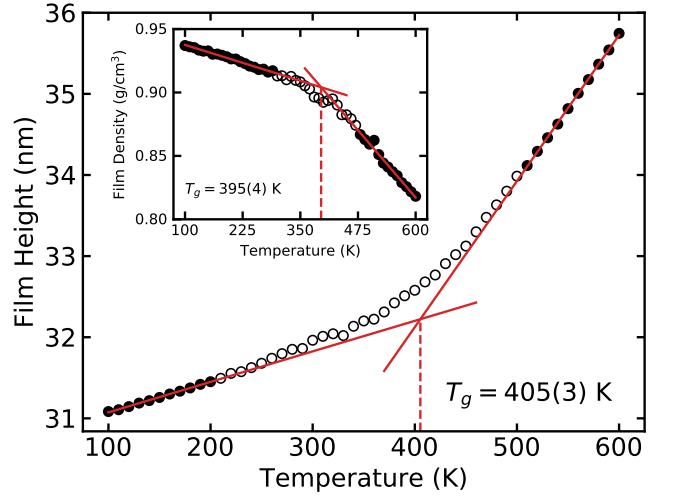


FIG. 2. Film height and density (inset) as a function of temperature during cooling of the PS-film. The glass transition temperature, T_g was found by fitting the linear regions (fitted points indicated by the filled symbols). Film edges were defined as the point where the density decreased to 50 % of the film center average.

film edge was defined to be the points where the density decreases to 50 % of the film center average. These values are within a few degrees from those reported by Zhou and Milner for a PS film also composed of 10mers of comparable thickness²⁰. From 600 K to 100 K, the film height decreased from 35.7 nm to 31.1 nm, and the density increased from 0.82 g/cm^3 to 0.94 g/cm^3 .

The motion of the two local structure vectors $\vec{v}(t)$ connecting the ortho atoms in the phenyl rings (adjacent to the tethering bond between the ring and the backbone) as well as adjacent CH_2 united atoms on the backbone were considered as indicators of polymer dynamics, as depicted in Figure 1. The autocorrelation function (ACF) of the second Legendre polynomial of the normalized vectors,

$$C(t) = \frac{3}{2} \left\langle [\hat{v}(t') \cdot \hat{v}(t' - t)]^2 \right\rangle_{t'} - \frac{1}{2}, \quad (11)$$

was used to determine the relaxation time, $\tau(z, T)$, defined to be time it takes for the average ACF to decay by a factor of $1/e$. The ACF was averaged by grouping each vector into 1 nm thick parallel laminae by distance to the nearest free surface.

IV. RESULTS

Figure 3 (top) and Figure 4 (top) present the layer-resolved rotational relaxation time of the phenyl rings and backbones for temperatures $400 \text{ K} \leq T \leq 500 \text{ K}$. The data represents an average over three independent trajectories of 0.5 μs to 1 μs duration. The relaxation times decrease significantly in layers less than

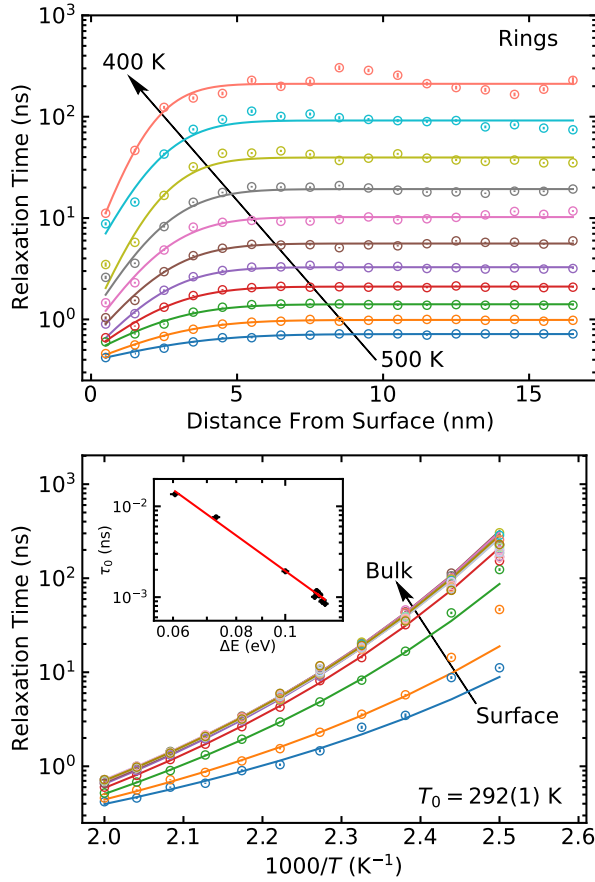


FIG. 3. Distance from surface (*top*) and temperature (*bottom*) dependence of the time of the autocorrelation function given by eq. (11) to decay to $1/e$, corresponding to the rotational motion of the polystyrene phenyl rings. Also shown are VFT fits to eq. (2) with a global VFT-temperature $T_0 = 292(1)$ K. The inset shows that the preexponential factor and activation barrier follow the Meyer-Neldel rule.

5 nm from the free surface, converging quickly with increasing depth to a temperature-dependent bulk value. The depth dependence was fit with the phenomenological form $\log \tau = c_0 + c_1 \text{erf}(z/z_0)$, as in Zhou and Milner²⁰, but with shared z_0 across all temperatures, yielding dynamical length scales of $z_0 = 3.23(2)$ nm and $z_0 = 2.85(4)$ nm for the rings and backbones, respectively. In our model, a freely varying z_0 produced length scales which did not vary appreciably in the temperature range studied. The length scales are comparable to that reported by Zhou and Milner²⁰ for the interfacial backbone relaxation and those found in bead-spring model simulations^{4,17,19,25}.

The bottom panels replot the same data in an Arrhenius representation and also show VFT fits, where the activation barrier and pre-exponential factors were allowed to vary with z but a single value of the VFT temperature T_0 was used over the entire data set. The VFT fits were performed only for $T \geq 410$ K, since the behavior has been observed to cross over to a purely Arrhenius

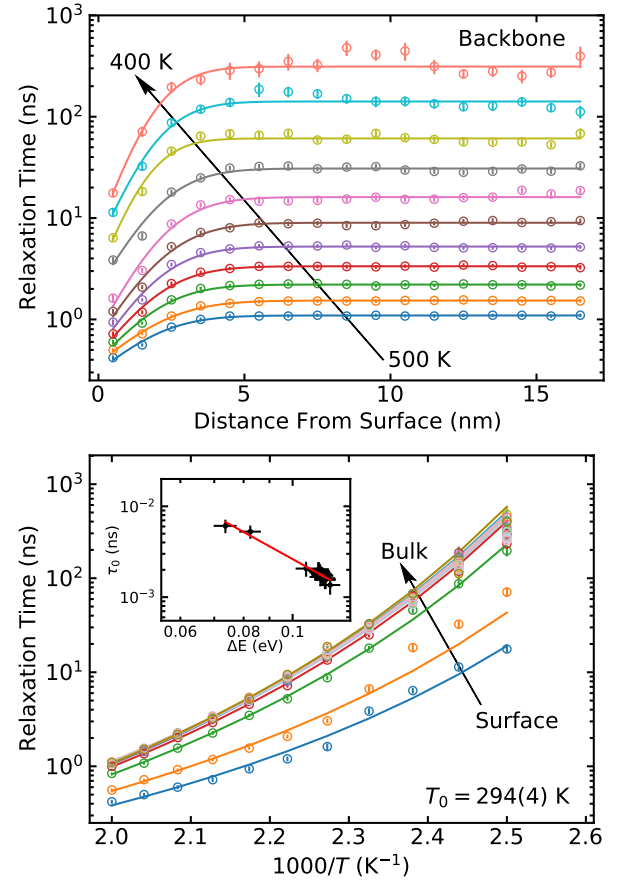


FIG. 4. Distance from surface (*top*) and temperature (*bottom*) dependence of the time of the autocorrelation function given by eq. (11) to decay to $1/e$, corresponding to the relaxation of the polystyrene backbone segments. Also shown are VFT fits to eq. (2) with a global VFT-temperature $T_0 = 294(4)$ K. The inset shows that the preexponential factor and activation barrier follow the Meyer-Neldel rule.

temperature dependence at temperatures near and below T_g ²⁶. In the supercooled regime, the data follows the VFT form reasonably well. The inset shows that the logarithm of the pre-exponential timescale $\tau_0(z)$ is proportional to the activation barrier $\Delta E(z)$, a behavior often referred to as the Meyer-Neldel rule^{27,28}. This can be interpreted as an entropy-enthalpy compensation effect and has also been observed in bead-spring models¹⁸. Results for the backbone motion mirror the behavior of the rings with longer relaxation times.

In order to test the validity of the explanations for near-surface relaxation, we plot in Figure 5 our data for PS films in the form $\log(\tau(T, z)/\tau_0(z))/\log(\tau_{\text{bulk}}(T)/\tau_0)$ vs z as suggested by eq. (3). This representation collapses curves for different T onto a master curve and thus reveals a temperature independent coupling exponent $f(z)$. A fit to an exponential form suggests a short interfacial length scale $\xi \simeq 1.5$ nm. For reference, the size of each monomer unit, as defined by the average distance between the CH_2 atoms along the backbone, is 0.27 nm.

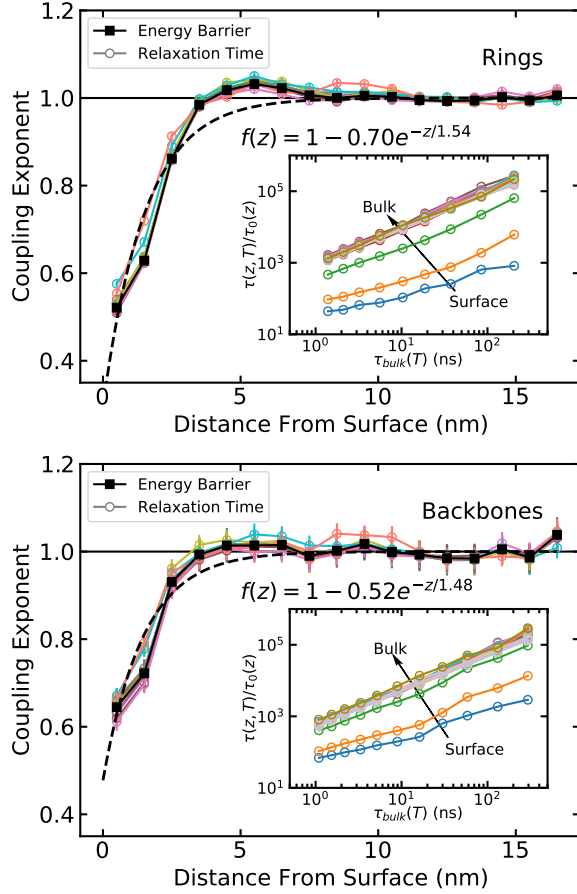


FIG. 5. Coupling exponent given by the logarithmic ratio of relaxation times $\log(\tau(T, z)/\tau_0(z))/\log(\tau_{bulk}(T)/\tau_0)$ (coloured, open) and ratio of activation barriers $\Delta E(z)/\Delta E_\infty$ (black, filled) from the VFT fits found in Figures 3 and 4 for rings (top) and backbones (bottom). The insets show the relaxation times vs bulk relaxation time. The dashed line indicates an exponential fit, as calculated from the relaxation times.

The insets show $\tau(z, T)/\tau_0(z)$ vs. $\tau_{bulk}(T)$ in double-logarithmic form, so that the slope of the curves is the coupling exponent. Obtaining straight lines, we conclude that $f(z)$ depends only on z and not on T . Our results are thus consistent with the proposal of Diaz-Vela, Hung, and Simmons⁸ that the activation barrier at distance z factorizes into distinct temperature- and depth-dependent parts,

$$\Delta E(z) = f(z)\Delta E_\infty. \quad (12)$$

As a further check of this relation, we can compare directly with the z -dependence of the activation barrier extracted from the VFT fits. The ratio $\Delta E(z)/\Delta E_\infty$ agrees strongly with the relaxation time data, and thus the form proposed in eq. (4), as shown in Figure 5.

The above results clearly support the picture of a depth-dependent activation barrier driving the interfacial relaxation dynamics⁹. In order to test the coopera-

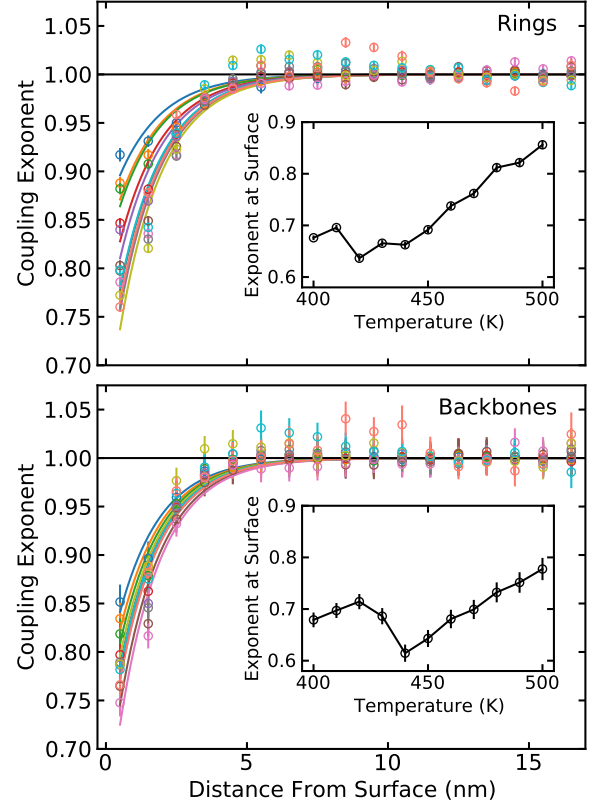


FIG. 6. Coupling exponent given by the logarithmic ratio of relaxation times $\log(\tau(T, z)/\tau_0)/\log(\tau_{bulk}(T)/\tau_0)$ for rings (top) and backbones (bottom) where the normalization τ_0 is taken as the bulk value and independent of z . Fits are to the exponential form as in Figure 5, with the characteristic length scale ξ fixed to the same as the corresponding fits in Figure 5. The inset shows the temperature dependence of the coupling exponent at $z = 0$.

tive strings prediction eq. (8), we examine in Figure 6 the data using a z -independent microscopic timescale τ_0 . In this representation, the curves do not fully collapse but include a residual temperature dependence that is captured by exponential fits using the temperature independent length scales found in Figure 5 (1.54 nm or 1.48 nm), but allowing for temperature-dependent prefactors. As a result, the temperature dependence is carried by a variation of the coupling exponent $0.6 < f(0) < 0.9$ at the surface (see insets). This result is at variance with the cooperative string model that anticipates complete decoupling at the interface¹⁵, i.e. $f(0) \sim 0$. It must be noted though that the cooperative string model is envisioned to apply at temperatures in the vicinity of T_0 , while our simulations are performed at higher temperatures. It is possible that $f(0)$ decreases further when the temperature is lowered towards the VFT temperature T_0 or when then polymer molecular weight increases.

In order to probe the role of cooperativity more directly, we need a measure of the scale of dynamical heterogeneity. One possibility is to consider the layer-

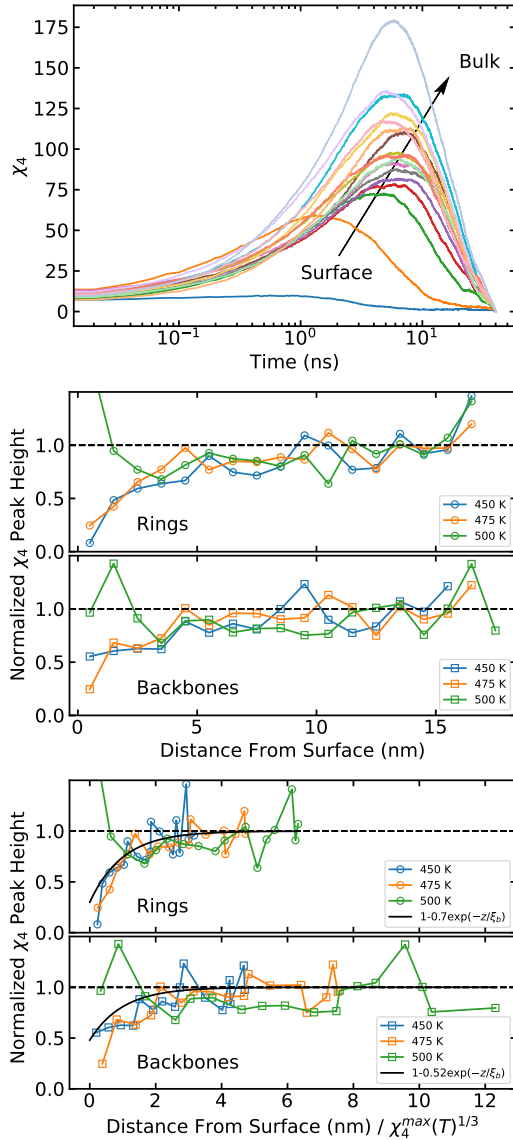


FIG. 7. (Top) Dynamical susceptibility $\chi_4(T = 450 \text{ K}, z, t)$ for the phenyl rings. (Center) Maximum of $\chi_4(T, z, t)$ vs. distance z from the free surface normalized by χ_4^{bulk} , which is computed as an average of the 5 layers furthest away from the surface. (Bottom) For comparison with the string model, we re-scale by $\chi_4^{max}(T)^{1/3}$, an estimate for $\xi_b(T)$. The surface point of the 500 K data (~ 1.8) was omitted for clarity. Black lines are produced from the fits in Figure 5.

resolved variance of the autocorrelation function or four-point dynamical susceptibility^{29,30}

$$\chi_4(T, z, t) = N_v(z) N_\tau(t) [\langle \bar{C}(z, t)^2 \rangle - \langle \bar{C}(z, t) \rangle^2], \quad (13)$$

where C is the ACF of an individual ring (backbone) vector as given by eq. (11), the overbar denotes an average over $N_v(z)$ ring (backbone) vectors in a given layer, $\langle \rangle$ an average over 100 simulation instances and $N_\tau(t)$ the number of time slices used in the calculation of the ACF for a given lag time t . $\chi_4(T, z, t)$ measures the fluctua-

tions of the total molecular mobility as given by the backbone or phenyl ring dynamics. It can also be viewed as a (spatial) integral over a four-point correlation function that measures how the dynamics at locations \mathbf{r}_1 and \mathbf{r}_2 over a time interval $t = t_1 - t_2$ are spatially correlated over a distance $\mathbf{r} = \mathbf{r}_1 - \mathbf{r}_2$. This function is shown for layers at different depths in the top panel of Figure 7 at temperature $T = 450 \text{ K}$ as a function of time. All curves at different layers z exhibit maxima at times that coincide with the layer-resolved relaxation times. The peak height can be interpreted as a correlation volume and thus proportional to the number of particles involved in a cooperative relaxation event. The middle panel plot this peak height $\chi_4^{max}(T)$ normalized by the bulk value in the center of the film vs distance from the surface. While the data at 500 K does not exhibit any trend, we clearly see a reduction of cooperativity at the lower temperatures 475 K and 450 K. In order to compare with the cooperative string model, we rescale z by the bulk cooperativity length $\xi_b(T)$, see eq. (7). In principle, this length scale could be extracted from the spatial decay of a four-point dynamical correlation function²⁹. Here, we use instead a simple estimate $\xi_b(T) \propto \chi_4^{max}(T)^{1/3}$, which is supported by simulations of a Lennard-Jones glass former³¹. The bottom panel of Figure 7 shows that plotting the normalized $\chi_4^{max}(T)$ data against $z/\chi_4^{max}(T)^{1/3}$ leads to a reasonable collapse of our (limited) data set. The form of this master curve is overall consistent with the behavior of the coupling exponent $f(z)$ computed in Figure 5 from the relaxation times (solid lines).

V. CONCLUSIONS

The relaxation times of backbone segments and phenyl rings at the surface of a freestanding PS film were examined with molecular dynamics simulation. The times τ are coupled to the bulk relaxation times via a power law relation with a temperature independent coupling exponent. These results extend previous bead-spring level simulations to a more detailed united atom model. The coupling exponent agrees well with the ratio of energy barriers extracted from VFT-fits, giving strong support to the notion that changes in the interfacial dynamics should be understood from interfacial changes in the activation free energy barrier. Moreover, the preexponential factors obey a Meyer-Neldel rule and thus exhibit considerable variation with depth below the free surface.

In the cooperative string model, the coupling exponent depends explicitly on temperature via the temperature dependence of the bulk cooperativity length. Our model does not show a strong variation of the interfacial length scale with temperature, and the coupling exponent remains well above zero at the free surface. In conceptual agreement with this approach, however, our calculations reveal a significant decrease of the dynamical four-point susceptibility near the surface. If one accepts this measure of dynamical heterogeneity as a good characteriza-

tion of cooperative motion, one can reconcile the coupling exponent with a normalized $\chi_4^{max}(z, T)$ ratio. Our results can be compared to a recent simulation study of the length L of mobile strings in supported bead-spring polymer films¹⁶. This work did not find any strong variation of L across the film except very close to the free surface, and concluded that collective motion does not vary spatially in any strong manner. It must be noted, however, that the characteristic string time that maximizes the dynamical string length is shorter than the alpha-relaxation time that marks the peak of $\chi_4(t, T)$. For this reason, the $\chi_4^{max}(z, T)$ parameter is more sensitive to slow particles as explained by Starr, Douglas, and Sastry³². Future work could clarify the relationship between different measures of cooperativity in greater detail.

VI. ACKNOWLEDGEMENTS

J.R. thanks the Alexander von Humboldt Foundation for financial support, and D.F. acknowledges the support from a SBQMI QuEST fellowship. This research was undertaken thanks, in part, to funding from the Canada First Research Excellence Fund, Quantum Materials and Future Technologies Program.

- ¹M. D. Ediger and J. A. Forrest, "Dynamics near free surfaces and the glass transition in thin polymer films: A view to the future," *Macromolecules* **47**, 471–478 (2014).
- ²J. A. Forrest and K. Dalnoki-Veress, "The glass transition in thin polymer films," *Adv. Colloid Interface Sci.* **94**, 167–195 (2001).
- ³J. S. Sharp and J. A. Forrest, "Free surfaces cause reductions in the glass transition temperature of thin polystyrene films," *Phys. Rev. Lett.* **91**, 235701 (2003).
- ⁴S. Peter, H. Meyer, and J. Baschnagel, "Thickness-dependent reduction of the glass-transition temperature in thin polymer films with a free surface," *J. Polym. Sci. Part B Polym. Phys.* **44**, 2951–2967 (2006).
- ⁵K. Paeng, S. F. Swallen, and M. D. Ediger, "Direct measurement of molecular motion in freestanding polystyrene thin films," *J. Am. Chem. Soc.* **133**, 8444–8447 (2011).
- ⁶I. McKenzie, Y. Chai, D. L. Cortie, J. A. Forrest, D. Fujimoto, V. L. Karner, R. F. Kiefl, C. D. P. Levy, W. A. Macfarlane, R. M. L. McFadden, G. D. Morris, M. R. Pearson, and S. Zhu, "Direct measurements of the temperature, depth and processing dependence of phenyl ring dynamics in polystyrene thin films by β -detected NMR," *Soft Matter* **14**, 7291–7544 (2018).
- ⁷I. McKenzie, C. R. Daley, R. F. Kiefl, C. D. P. Levy, W. A. MacFarlane, G. D. Morris, M. R. Pearson, D. Wang, and J. A. Forrest, "Enhanced high-frequency molecular dynamics in the near-surface region of polystyrene thin films observed with b-NMR," *Soft Matter* **11**, 1755–1761 (2015).
- ⁸D. Diaz-Vela, J.-H. Hung, and D. S. Simmons, "Temperature-independent rescaling of the local activation barrier drives free surface nanoconfinement effects on segmental-scale translational dynamics near t_g ," *ACS Macro Lett.* **7**, 1295–1301 (2018).
- ⁹K. S. Schweizer and D. S. Simmons, "Progress towards a phenomenological picture and theoretical understanding of glassy dynamics and vitrification near interfaces and under nanoconfinement," *J. Chem. Phys.* **151**, 240901 (2019).
- ¹⁰S. Mirigian and K. S. Schweizer, "Communication: Slow relaxation, spatial mobility gradients, and vitrification in confined films," *J. Chem. Phys.* **141**, 161103 (2014).
- ¹¹A. D. Phan and K. S. Schweizer, "Dynamic gradients, mobile layers, t_g shifts, role of vitrification criterion, and inhomogeneous decoupling in free-standing polymer films," *Macromolecules* **51**, 6063–6075 (2018).
- ¹²A. D. Phan and K. S. Schweizer, "Influence of longer range transfer of vapor interface modified caging constraints on the spatially heterogeneous dynamics of glass-forming liquids," *Macromolecules* **52**, 5192–5206 (2019).
- ¹³A. D. Phan and K. S. Schweizer, "Theory of the spatial transfer of interface-nucleated changes of dynamical constraints and its consequences in glass-forming films," *J. Chem. Phys.* **150**, 044508 (2019).
- ¹⁴A. D. Phan and K. S. Schweizer, "Theory of spatial gradients of relaxation, vitrification temperature and fragility of glass-forming polymer liquids near solid substrates," *ACS Macro Lett.* **9**, 448–453 (2020).
- ¹⁵T. Salez, J. Salez, K. Dalnoki-Veress, E. Raphaël, and J. A. Forrest, "Cooperative strings and glassy interfaces," *Proc. Natl. Acad. Sci.* **112**, 8227–8231 (2015).
- ¹⁶W. Zhang, F. W. Starr, and J. F. Douglas, "Collective motion in the interfacial and interior regions of supported polymer films and its relation to relaxation," *J. Phys. Chem. B* **123**, 5935–5941 (2019).
- ¹⁷R. J. Lang and D. S. Simmons, "Interfacial Dynamic Length Scales in the Glass Transition of a Model Freestanding Polymer Film and Their Connection to Cooperative Motion," *Macromolecules* **46**, 9818–9825 (2013).
- ¹⁸P. Z. Hanakata, J. F. Douglas, and F. W. Starr, "Interfacial mobility scale determines the scale of collective motion and relaxation rate in polymer films," *Nat. Commun.* **5**, 4163 (2014).
- ¹⁹A. Shavit and R. A. Riggelman, "Physical Aging, the Local Dynamics of Glass-Forming Polymers under Nanoscale Confinement," *J. Phys. Chem. B* **118**, 9096–9103 (2014).
- ²⁰Y. Zhou and S. T. Milner, "Short-Time Dynamics Reveals T_g Suppression in Simulated Polystyrene Thin Films," *Macromolecules* **50**, 5599–5610 (2017).
- ²¹B. Vorselaars, A. V. Lyulin, and M. A. J. Michels, "Development of heterogeneity near the glass transition: Phenyl-ring-flip motions in polystyrene," *Macromolecules* **40**, 6001–6011 (2007).
- ²²I. McKenzie, M. Harada, R. F. Kiefl, C. D. P. Levy, W. A. Macfarlane, G. D. Morris, S.-I. Ogata, M. R. Pearson, and J. Sugiyama, " β - α NMR Measurements of Lithium Ion Transport in Thin Films of Pure and Lithium-Salt-Doped Poly(ethylene oxide)," *J. Am. Chem. Soc.* **136**, 7833–7836 (2014).
- ²³B. A. Pazmiño Betancourt, J. F. Douglas, and F. W. Starr, "String model for the dynamics of glass-forming liquids," *J. Chem. Phys.* **140**, 204509 (2014).
- ²⁴S. Plimpton, "Fast Parallel Algorithms for Short-Range Molecular Dynamics," *J. Comput. Phys.* **117**, 1–19 (1995).
- ²⁵D. M. Sussman, S. S. Schoenholz, E. D. Cubuk, and A. J. Liu, "Disconnecting structure and dynamics in glassy thin films," *Proc. Natl. Acad. Sci.* **114**, 10601 (2017).
- ²⁶A. V. Lyulin, N. K. Balabaev, and M. Michels, "Correlated segmental dynamics in amorphous atactic polystyrene: A molecular dynamics simulation study," *Macromolecules* **35**, 9595–9604 (2002).
- ²⁷W. v. Meyer and H. Neldel, "Relation between the energy constant and the quantity constant in the conductivity-temperature formula of oxide semiconductors," *Z. tech. Phys.* **18**, 588–593 (1937).
- ²⁸A. Yelon, B. Movaghar, and H. M. Branz, "Origin and consequences of the compensation (Meyer-Neldel) law," *Phys. Rev. B* **46** (1992).
- ²⁹N. LaÅdeviÅC, F. W. Starr, T. B. SchrÅyder, and S. C. Glotzer, "Spatially heterogeneous dynamics investigated via a time-dependent four-point density correlation function," *J. Chem. Phys.* **119**, 7372–7387 (2003).
- ³⁰L. Berthier, "Dynamic heterogeneity in amorphous materials," *Physics* **4**, 42 (2011).

³¹E. Flenner and G. Szamel, “Dynamic heterogeneity in a glass forming fluid: Susceptibility, structure factor, and correlation length,” *Phys. Rev. Lett.* **105**, 217801 (2010).

³²F. W. Starr, J. F. Douglas, and S. Sastry, “The relationship of dynamical heterogeneity to the Adam-Gibbs and random first-order transition theories of glass formation,” *J. Chem. Phys.* **138**, 12A541 (2013).